A vorticity method for the solution of natural convection flows in enclosures

Marc S. Ingber
Department of Mechanical Engineering, University of New Mexico, Albuquerque, New Mexico, USA

Received December 2001
Revised September 2002
Accepted January 2003

Keywords *Convection, Boundary elements methods, Finite element analysis*

Abstract *Vorticity formulations for the incompressible Navier-Stokes equations have certain advantages over primitive-variable formulations including the fact that the number of equations to be solved is reduced through the elimination of the pressure variable, identical satisfaction of the incompressibility constraint and the continuity equation, and an implicitly higher-order approximation of the velocity components. For the most part, vorticity methods have been used to solve exterior isothermal problems. In this research, a vorticity formulation is used to study the natural convection flows in differentially-heated enclosures. The numerical algorithm is divided into three steps: two kinematic steps and one kinetic step. The kinematics are governed by the generalized Helmholtz decomposition (GHD) which is solved using a boundary element method (BEM) whereas the kinetics are governed by the vorticity equation which is solved using a finite element method (FEM). In the first kinematic step, vortex sheet strengths are determined from a novel Galerkin implementation of the GHD. These vortex sheet strengths are used to determine Neumann boundary conditions for the vorticity equation. (The thermal boundary conditions are already known.) In the second kinematic step, the interior velocity field is determined using the regular (non-Galerkin) form of the GHD. This step, in a sense, linearizes the convective acceleration terms in both the vorticity and energy equations. In the third kinetic step, the coupled vorticity and energy equations are solved using a Galerkin FEM to determine the updated values of the vorticity and thermal fields. Two benchmark problems are considered to show the robustness and versatility of this formulation including natural convection in an 8×1 differentially-heated enclosure at a near critical Rayleigh number.*

1. Introduction

Vorticity formulations have been used to analyze a variety of isothermal, incompressible viscous flow problems including interior flows in driven cavities (Ingber and Kempka, 2001; Ramšak and Škerget, 1999; Young *et al.*, 2000) and Couette devices (Machane *et al.*, 2000) and exterior flows over cylinders (El-Refaee, 1994; Koumoutsakos and Leonard, 1995) and airfoils (Tuncer *et al.*, 1990; Wang and Wu, 1990). Far fewer applications of vorticity formulations have appeared in the literature for non-isothermal flows. Škerget and coworkers have used vorticity formulations to study both natural convection in porous media (Jeel *et al.*, 1999) and differentially-heated enclosures (Ramšak and Škerget, 1999).

Vorticity formulations for the incompressible Navier-Stokes equations have distinct advantages over velocity-pressure formulations. These advantages

International Journal of Numerical Methods for Heat & Fluid Flow
Vol. 13 No. 6, 2003
pp. 655-671

0961-5539
DOI 10.1108/09615530310498367

remain largely untapped; however, since questions concerning how to determine accurate boundary conditions for vorticity formulations have posed difficult problems (Ostrikov and Zhmulin, 1994). Boundary conditions are typically given in terms of prescribed velocities, but boundary conditions in terms of vorticity are required for vorticity formulations. Thus, it is necessary to deduce vorticity boundary conditions from not only the velocity boundary conditions, but also from the vorticity field in the domain.

In a recent paper, Ingber and Kempka (2001) discussed a Galerkin implementation of the generalized Helmholtz decomposition (GHD) to determine accurate boundary conditions for either the boundary vorticity (yielding a Dirchlet problem) or the vorticity flux (yielding a Neumann problem). They showed that the Galerkin implementation of the GHD yielded vorticity boundary conditions that resulted in the velocity boundary conditions being satisfied in orders of magnitude better than by using the more traditional point-collocation implementation of the GHD.

The ultimate purpose of resolving the issues of accurate specification of the vorticity boundary conditions is to implement a method for determining these boundary conditions into a numerical algorithm based on the vorticity form of the Navier-Stokes equations. Ingber and Kempka (2001) coupled a Galerkin finite element method (FEM) for solving the vorticity equation with the Galerkin GHD to determine appropriate boundary conditions to solve a variety of internal and external isothermal viscous fluid flow problems. In the current research, this vorticity approach is extended to two-dimensional (2D) flows of Boussinesque fluids. The accuracy of the formulation is demonstrated by considering the natural convection flows in differentially-heated enclosures.

2. Numerical formulation

The 2D non-dimensional governing equations for the time-dependent thermal convection problem are the incompressible Navier-Stokes equations, conservation of mass, and the energy equation written in terms of temperature:

$$\frac{\partial \vec{u}}{\partial t} + \vec{u} \cdot \nabla \vec{u} = -\nabla P + \sqrt{\frac{\mathrm{Pr}}{\mathrm{Ra}}} \nabla^2 \vec{u} + \vec{j}\theta, \tag{1}$$

$$\nabla \cdot \vec{u} = 0, \tag{2}$$

and

$$\frac{\partial \theta}{\partial t} + \vec{u} \cdot \nabla \theta = \frac{1}{\sqrt{\mathrm{RaPr}}} \nabla^2 \theta, \tag{3}$$

where $\vec{u}$, P, and θ are the non-dimensional velocity, pressure, and temperature fields, respectively, Ra is the Rayleigh number, Pr is the Prandtl number, and $\vec{j}$ is the unit vector in the y-direction. The non-dimensional equations are

obtained using a characteristic width, W, of the enclosure, velocity $U = \sqrt{g\beta W \Delta T}$, time scale $\tau = W/U$, and pressure $\bar{P} = \rho U^2$. Here, $\Delta T = T_h - T_c$ is the difference between the temperature of the hot wall, T_h, and the cold wall, T_c, ρ is the mass density, g is the gravitational acceleration, and β is the coefficient of thermal expansion. The non-dimensional temperature θ is defined by

$$\theta = \frac{T - T_r}{\Delta T}, \tag{4}$$

where the reference temperature is given by

$$T_r = \frac{T_h + T_c}{2}. \tag{5}$$

The Rayleigh number, Ra, and Prandtl number, Pr, are given by

$$\mathrm{Ra} = \frac{g\beta \Delta T W^3}{\nu\alpha}; \qquad \mathrm{Pr} = \frac{\nu}{\alpha},$$

where α is the thermal diffusivity.

To express the momentum equation in terms of the vorticity, $\omega = \nabla \times \vec{u}$, the curl of equation (1) is taken to yield

$$\frac{\partial \vec{\omega}}{\partial t} + (\vec{u} \cdot \nabla)\vec{\omega} = \nu \nabla^2 \vec{\omega} + \frac{\partial \theta}{\partial x}. \tag{6}$$

Hence, the governing equations in terms of vorticity consists of equations (3) and (6) only since the continuity equation (equation (2)) is identically satisfied by the vorticity formulation.

In the course of solving the governing system of equations, the velocity field, $\vec{u}$, must be determined from the vorticity field, $\vec{\omega}$, and the creation of vorticity on the boundary must be determined from the velocity boundary conditions. In the present formulation, determining both the interior velocity field and the creation of vorticity on the boundary are accomplished in an unified manner using the GHD.

The GHD is a classical kinematical statement decomposing the vorticity field into a solenoidal and rotational part (Morino, 1986). Derivations and discussions of the GHD can be found in Hribersek and Skerget, 1996; Kempka *et al.*, 1996; Meir and Schmidt, 1996; Morino, 1986; Wu and Thompson, 1973). For an incompressible fluid in 2D, the GHD is given by

$$\eta(\vec{x})[\vec{u}(\vec{x}) - \vec{\gamma}(\vec{x}) \times \vec{n}(\vec{x})] = \int_{\Omega} \frac{\vec{\omega}(\vec{y}) \times \vec{r}(\vec{x},\vec{y})}{r^2(\vec{x},\vec{y})} \, d\Omega(\vec{y}) + \int_{\Gamma} \frac{[(\vec{u}(\vec{y}) - \vec{\gamma}(\vec{y}) \times \vec{n}(\vec{y})) \times \vec{n}(\vec{y})] \times \vec{r}(\vec{x},\vec{y})}{r^2(\vec{x},\vec{y})} \, d\Gamma(\vec{y}) - \int_{\Gamma} \frac{[\vec{u}(\vec{y}) \cdot \vec{n}(\vec{y})]\vec{r}(\vec{x},\vec{y})}{r^2(\vec{x},\vec{y})} \, d\Gamma(\vec{y}), \tag{7}$$

where $\vec{n}$ is the unit normal vector on the boundary (pointing away from the fluid), $\vec{r} = \vec{x} - \vec{y}$, $r = |\vec{r}|$, Ω represents the 2D domain, Γ is the boundary of Ω, and $\vec{\gamma}$ represents the vortex sheet strengths along the boundary. The coefficient η is a function of the location of the field point $\vec{x}$. In particular, for field points on smooth portions of the boundary, $\eta = \pi/2$.

The GHD is valid only for certain kinematically admissible interior vorticity fields, $\vec{\omega}$, and velocity boundary conditions. For example, assume that equation (7) is satisfied at a given time, τ, and consider an explicit time integration of the vorticity and energy equations. After the vorticity field has been transported, but without properly considering the production and transport of vorticity at the boundary, equation (7) is no longer generally satisfied. Kinematic compatibility is re-established by solving equation (7) for the unknown vortex sheet strengths which represents the vorticity creation during a given time step (Ingber and Kempka, 2001; Lighthill, 1963).

3. Numerical implementation

A Galerkin implementation of the GHD for determining the vortex sheet strengths using a traditional boundary element discretization is presented first. Next, a Galerkin FEM is presented for solving the vorticity form of the governing kinetic equations (equations (6) and (3)). Finally, an outline of the numerical algorithm for analyzing the natural convection flows in enclosures is presented.

3.1 Galerkin approximation of the GHD

The domain Ω is discretized into interior integration cells and the boundary of the domain Γ is discretized into boundary elements. The interior integration cells are identical to the finite elements used for the solution of the vorticity and energy equations. Furthermore, as discussed later, the approximation of the vorticity ω used to evalaute the domain integral in the GHD is based on the standard finite element nodal basis functions. Hence, the interior integration cells will be refered to in this section as finite elements. For simplicity, let $\vec{t}$ represent $\vec{u} - \vec{\gamma} \times \vec{n}$. Within the eth finite element Ω_e, the jth component of $\vec{\omega}$ is approximated as

$$\omega_j^e(\vec{y}) = \sum_{l=1}^{4} \omega_{lj}^e S_l(\vec{y}), \tag{8}$$

where ω_{lj}^e represents the value of the jth component of $\vec{\omega}$ at the lth node within the eth finite element and S_l represents the bilinear Lagrangian shape function associated with the finite element. Similarly, within the eth boundary element, Γ_e, the jth component of $\vec{t}$ is approximated as

$$t_j^e(\vec{y}) = \sum_{l=1}^{2} t_{lj}^e N_l(\vec{y}) \tag{9}$$

where, in this case, t_{lj}^e represents the value of the jth component of $\vec{t}$ at the lth node within the eth boundary element and N_l represents the linear Lagrangian shape function associated with the boundary element.

Substituting equations (8) and (9) into equation (7), the discretized form of the GHD can be written using indicial notation as

$$\eta(\vec{x})t_i(\vec{x}) = \sum_{e=1}^{\mathrm{NFE}} \int_{\Omega_e} \frac{e_{ijk}\omega_{lj}S_l(\vec{y})d_k}{d_r d_r}\,\mathrm{d}\Omega + \sum_{e=1}^{\mathrm{NBE}} \int_{\Gamma_e} \frac{e_{imp}e_{mjk}t_{lj}^e N_l(\vec{y})n_k d_p}{d_r d_r}\,\mathrm{d}\Gamma - \sum_{e=1}^{\mathrm{NBE}} \int_{\Gamma_e} \frac{t_{lj}^e N_l(\vec{y})n_j d_i}{d_r d_r}\,\mathrm{d}\Gamma, \tag{10}$$

where e_{ijk} is the unit alternating tensor, NFE represents the number of finite elements, NBE represents the number of boundary elements, and $d_i = x_i - y_i$ where $\vec{x} = (x_1, x_2)$ and $\vec{y} = (y_1, y_2)$.

Using the properties of the unit alternating tensor, this equation can be rewritten as

$$\eta(\vec{x})t_i(\vec{x}) = \sum_{g=1}^{\mathrm{NFE}} \int_{\Omega_g} \frac{e_{ijk}\omega_{lj}^g S_l d_k}{d_r d_r}\,\mathrm{d}\Omega + \sum_{e=1}^{\mathrm{NBE}} \int_{\Gamma_e} \frac{t_{lk}^e N_l d_k n_i - t_{li}^e N_l d_k n_k - t_{lk}^e N_l d_i n_k}{d_r d_r}\,\mathrm{d}\Gamma. \tag{11}$$

The term $\eta(\vec{x})t_i(\vec{x})$ can be incorporated directly into the boundary integral by considering rigid body arguments (Brebbia and Dominguez, 1989; Ingber and Kempka, 2001). That is, by considering t_i to be a constant, it can be shown that (Ingber and Kempka, 2001)

$$\int_{\Gamma} \frac{d_2 n_1 - d_1 n_2}{d_r d_r} \, \mathrm{d}\Gamma = 0, \tag{12}$$

and

$$\eta(\vec{x}) = -\int_{\Gamma} \frac{d_k n_k}{d_r d_r} \, \mathrm{d}\Gamma. \tag{13}$$

Using equations (12) and (13), the left hand side of equation (11) can be incorporated into the right hand side. The resulting integral equation is given by

$$0 = \sum_{g=1}^{\mathrm{NFE}} \int_{\Omega_g} \frac{e_{ijk}\omega_{lj}^{g} S_1(\vec{y}) d_k}{d_r d_r} \, \mathrm{d}\Omega + \sum_{e=1}^{\mathrm{NBE}} \int_{\Gamma_e} \frac{[t_{lk}^{e} N_1(\vec{y}) - t_i(\vec{x})](d_k n_i - d_i n_k) - [t_{li}^{e} N_1(\vec{y}) - t_i(\vec{x})] d_k n_k}{d_r d_r} \, \mathrm{d}\Gamma. \tag{14}$$

This formulation not only has the advantage of not having to evaluate $\eta(\vec{x})$ explicitly, but also regularizes the Cauchy Principal Value integral on the right hand side of equation (11).

To obtain a Galerkin approximation, equation (14) is multiplied by the shape functions, $N_m(\vec{x})$ and integrated over the boundary Γ. Assuming that $N_m(\vec{x})$ has support within the fth boundary element and, within that element

$$t_k(\vec{x}) \,|_{\Gamma_f} = t_{lk}^{f} N_1(\vec{x}),$$

the discretized Galerkin approximation for the GHD is given by

$$0 = \sum_{g=1}^{\mathrm{NFE}} \int_{\Gamma_f} N_m(\vec{x}) \int_{\Omega_g} \frac{e_{ijk}\omega_{lj}^{g} S_1(\vec{y}) d_k}{d_r d_r} \, \mathrm{d}\Omega + \sum_{e=1}^{\mathrm{NBE}} \int_{\Gamma_f} N_m(\vec{x}) \int_{\Gamma_e} \frac{\left[t_{lk}^{e} N_1(\vec{y}) - t_{li}^{f} N_1(\vec{x})\right](d_k n_i - d_i n_k)}{d_r d_r} \, \mathrm{d}\Gamma - \sum_{e=1}^{\mathrm{NBE}} \int_{\Gamma_f} N_m(\vec{x}) \int_{\Gamma_e} \frac{\left[t_{li}^{e} N_1(\vec{y}) - t_{li}^{f} N_1(\vec{x})\right] d_k n_k}{d_r d_r} \, \mathrm{d}\Gamma. \tag{15}$$

3.2 Galerkin FEM solution of the governing equations

The Galerkin FEM used to solve the governing equations for natural convection flows is outlined in this subsection. Multiplying the 2D vorticity equation (equation (6)) and the energy equation (equation (3)) by a weighting function, w, and integrating over the domain yields

$$\int_\Omega w\frac{\partial \omega}{\partial t}\,\mathrm{d}\Omega + \int_\Omega \left(u_x w\frac{\partial \omega}{\partial x} + u_y w\frac{\partial \omega}{\partial y}\right)\mathrm{d}\Omega - \int_\Omega \sqrt{\frac{\mathrm{Pr}}{\mathrm{Ra}}}\left(w\frac{\partial^2 \omega}{\partial x^2} + w\frac{\partial^2 \omega}{\partial y^2}\right)\mathrm{d}\Omega - \int_\Omega w\frac{\partial \theta}{\partial x}\,\mathrm{d}\Omega = 0, \tag{16}$$

and

$$\int_\Omega w\frac{\partial \theta}{\partial t}\,\mathrm{d}\Omega + \int_\Omega \left(u_x w\frac{\partial \theta}{\partial x} + u_y w\frac{\partial \theta}{\partial y}\right)\mathrm{d}\Omega - \int_\Omega \sqrt{\frac{1}{\mathrm{PrRa}}}\left(w\frac{\partial^2 \theta}{\partial x^2} + w\frac{\partial^2 \omega}{\partial y^2}\right)\mathrm{d}\Omega = 0, \tag{17}$$

where u_x and u_y are the components of the velocity vector $\vec{u}$. Integrating the second-order terms by parts (applying Green's theorem), the weak forms of the above equations are written as

$$\int_\Omega w\frac{\partial \omega}{\partial t}\,\mathrm{d}\Omega + \int_\Omega \left(u_x w\frac{\partial \omega}{\partial x} + u_y w\frac{\partial \omega}{\partial y}\right)\mathrm{d}\Omega + \int_\Omega \sqrt{\frac{\mathrm{Pr}}{\mathrm{Ra}}}\left(\frac{\partial \omega}{\partial x}\frac{\partial w}{\partial x} + \frac{\partial \omega}{\partial y}\frac{\partial w}{\partial y}\right)\mathrm{d}\Omega + \int_\Omega w\frac{\partial \theta}{\partial x}\,\mathrm{d}\Omega = \int_\Gamma w q_n\,\mathrm{d}\Gamma, \tag{18}$$

and

$$\int_\Omega w\frac{\partial \theta}{\partial t}\,\mathrm{d}\Omega + \int_\Omega \left(u_x w\frac{\partial \theta}{\partial x} + u_y w\frac{\partial \theta}{\partial y}\right)\mathrm{d}\Omega + \int_\Omega \sqrt{\frac{1}{\mathrm{PrRa}}}\left(\frac{\partial \theta}{\partial x}\frac{\partial w}{\partial x} + \frac{\partial \theta}{\partial y}\frac{\partial w}{\partial y}\right)\mathrm{d}\Omega = 0. \tag{19}$$

As shown by Ingber and Kempka (2001), the normal flux of vorticity is related to the vortex sheet strengths by

$$q_n = \frac{\partial \omega}{\partial n} = \frac{\gamma}{\nu \Delta t}. \tag{20}$$

Further, since temperature is specified on the lateral boundary of the enclosure and the top and bottom of the enclosure is insolated, no boundary integral appears in equation (18).

The weak forms are discretized by subdividing the domain Ω into finite elements and subdividing the boundary Γ into boundary elements. Again, using isoparametric bilinear Lagrangian interpolation for the finite elements and linear interpolation for the boundary elements, the weak forms can be written in discrete form as

$$\sum_{i=1}^{\mathrm{NBE}} w_i^e \int_{\Gamma_e} N_i^e \frac{N_k^e}{\Delta t}\,\mathrm{d}\Gamma\,\gamma_k^e = \sum_{e=1}^{\mathrm{NFE}} w_i^e \int_{\Omega^e} S_i S_j\,\mathrm{d}\Omega\,\frac{\mathrm{d}\omega_j^e}{\mathrm{d}t} + \sum_{e=1}^{\mathrm{NFE}} w_i^e \sqrt{\frac{\mathrm{Pr}}{\mathrm{Ra}}} \int_{\Omega_e} \left(\frac{\partial S_i}{\partial x}\frac{\partial S_j}{\partial x} + \frac{\partial S_i}{\partial y}\frac{\partial S_j}{\partial y}\right)\mathrm{d}\Omega\,\omega_j^e + \sum_{e=1}^{\mathrm{NFE}} w_i^e \int_{\Omega_e} S_i \frac{\partial S_j}{\partial x}\,\mathrm{d}\Omega\,\theta_j^e + \sum_{e=1}^{\mathrm{NFE}} w_i^e \int_{\Omega_e} \left(S_i \frac{\partial S_j}{\partial x} u_{xk}^e S_k + S_i \frac{\partial S_j}{\partial y} u_{yk}^e S_k\right)\mathrm{d}\Omega\,\omega_j^e, \tag{21}$$

and

$$0 = \sum_{e=1}^{\mathrm{NFE}} w_i^e \int_{\Omega^e} S_i S_j\,\mathrm{d}\Omega\,\frac{\mathrm{d}\theta_j^e}{\mathrm{d}t} + \sum_{e=1}^{\mathrm{NFE}} w_i^e \sqrt{\frac{\mathrm{Pr}}{\mathrm{Ra}}} \int_{\Omega_e} \left(\frac{\partial S_i}{\partial x}\frac{\partial S_j}{\partial x} + \frac{\partial S_i}{\partial y}\frac{\partial S_j}{\partial y}\,\mathrm{d}\Omega\right)\mathrm{d}\Omega\,\theta_j^e + \sum_{e=1}^{\mathrm{NFE}} w_i^e \int_{\Omega_e} \left(S_i \frac{\partial S_j}{\partial x} u_{xk}^e S_k + S_i \frac{\partial S_j}{\partial y} u_{yk}^e S_k\right)\mathrm{d}\Omega\,\theta_j^e, \tag{22}$$

where w_i^e, ω_i^e, u_{xi}^e, u_{yi}^e, and θ_j^e represent the values of w, ω, u_x, u_y, and θ, respectively, at the ith node within the eth finite element and γ_i^e represents the value of γ at the ith node within the eth boundary element. For convenience, the element capacitance matrices, element stiffness matrices, and element load vectors are defined by

$$(C^e)_{ij} = \int_{\Omega_e} S_i^e S_j^e \, \mathrm{d}\Omega, \tag{23}$$

$$(K_x^e)_{ij} = \int_{\Omega_e} \frac{\partial S_i^e}{\partial x} \frac{\partial S_j^e}{\partial x} \, \mathrm{d}\Omega, \tag{24}$$

$$(K_y^e)_{ij} = \int_{\Omega_e} \frac{\partial S_i^e}{\partial y} \frac{\partial S_j^e}{\partial y} \, \mathrm{d}\Omega, \tag{25}$$

$$(K_u^e)_{ij} = \sum_{k=1}^{4} u_{xk}^e \int_{\Omega_e} S_i^e \frac{\partial S_j^e}{\partial x} S_k^e \, \mathrm{d}\Omega, \tag{26}$$

$$(K_v^e)_{ij} = \sum_{k=1}^{4} u_{yk}^e \int_{\Omega_e} S_i^e \frac{\partial S_j^e}{\partial y} S_k^e \, \mathrm{d}\Omega, \tag{27}$$

$$(K_\theta^e)_{ij} = \int_{\Omega_e} S_i^e \frac{\partial S_j^e}{\partial x} \, \mathrm{d}\Omega, \tag{28}$$

$$(F^e)_i = \frac{1}{\Delta t} \gamma_k^e \int_{\Gamma_e} N_i^e N_j^e \, \mathrm{d}\Gamma. \tag{29}$$

After assembly, the discretized weak forms can be written in the following convenient form

$$[K_{\mathrm{th}}]\{\theta\} + \left[K_x + K_y + \sqrt{\frac{\mathrm{Pr}}{\mathrm{Ra}}}(K_u + K_v)\right]\{\omega\} + [C]\{\dot{\omega}\} = \{F\}, \tag{30}$$

and

$$\left[K_x + K_y + \sqrt{\frac{1}{\mathrm{PrRa}}}(K_u + K_v)\right]\{\theta\} + [C]\{\dot{\theta}\} = 0. \tag{31}$$

The discretized equation set (equation (30) and equation (31) is inherently non-linear since the matrices K_u and K_v contain the unknown velocity field components. In the current implementation, the velocity components in those stiffness matrices are evaluated using equation (7). Time is discretized using an Euler explicit integrator resulting in a first-order accurate method in time.

3.3 Outline of the numerical algorithm

The numerical algorithm for solving the equations governing natural convection flows in enclosures is outlined. First, the vortex sheet strengths are calculated using the tangential component of the Galerkin form of the GHD (equation (15)). The vortex sheet strengths are then related to the normal flux of vorticity at the boundary using equation (20). Next, the internal velocities at the finite element interior nodes are calculated using the regular form of the GHD (equation (7)) allowing the evaluation of the stiffness matrices $(K_u^e)_{ij}$ and $(K_v^e)_{ij}$. Finally, to complete the time step, the vorticity and temperature fields are transported by solving the explicit form of the discretized finite element equations (equation (30) and (31)). After the explicit convection of vorticity, the flow field is again kinematically incompatible without incorporating the newly formed vortex sheet strengths at the boundary. This kinematic incompatibility is resolved by going back to the first step, thus initiating the next time step.

In the current implementation of the numerical algorithm, both the discretized FEM and the GHD equations are solved by using an LU solver. The decompositions are done outside the time loop. Further, all integrals for evaluating the interior velocities are also performed outside the time loop. Hence, within the time loop, the majority of calculation is matrix-vector multiplication and back substitution.

4. Numerical results

Two benchmark problems are considered to show the capabilities of the current vorticity formulation. The first benchmark problem is natural convection in a differentially-heated square enclosure at $\mathrm{Pr} = 0.71$ and $\mathrm{Ra} = 1{,}000$. The second benchmark problem is natural convection in an 8×1 differentially-heated enclosure at $\mathrm{Pr} = 0.71$ and $\mathrm{Ra} = 3.1 \times 10^5$. All simulations except for the finest mesh in the second benchmark were started from an initially quiescent state with the temperatures at the left and right walls impulsively changed to $\theta = 0.5$ and -0.5, respectively. The simulation using the finest mesh for the second benchmark was started from interpolated results of the medium mesh after quasi-steady state had been achieved.

4.1 Benchmark problem 1

Only the steady state results are presented for the square enclosure in the first benchmark problem even though the simulation was run from the initial conditions through the transient. A 31×31 and 41×41 uniform finite element mesh and non-dimensional time step of 0.001 was used. Steady state was achieved within 15 s.

Contour plots for the u-component (horizontal) of velocity, v-component (vertical) of velocity, temperature and vorticity at steady state determined using the 31×31 finite element mesh is shown in Figure 1. De Vahl Davis and Jones (1983) compiled numerical results from a number of invited

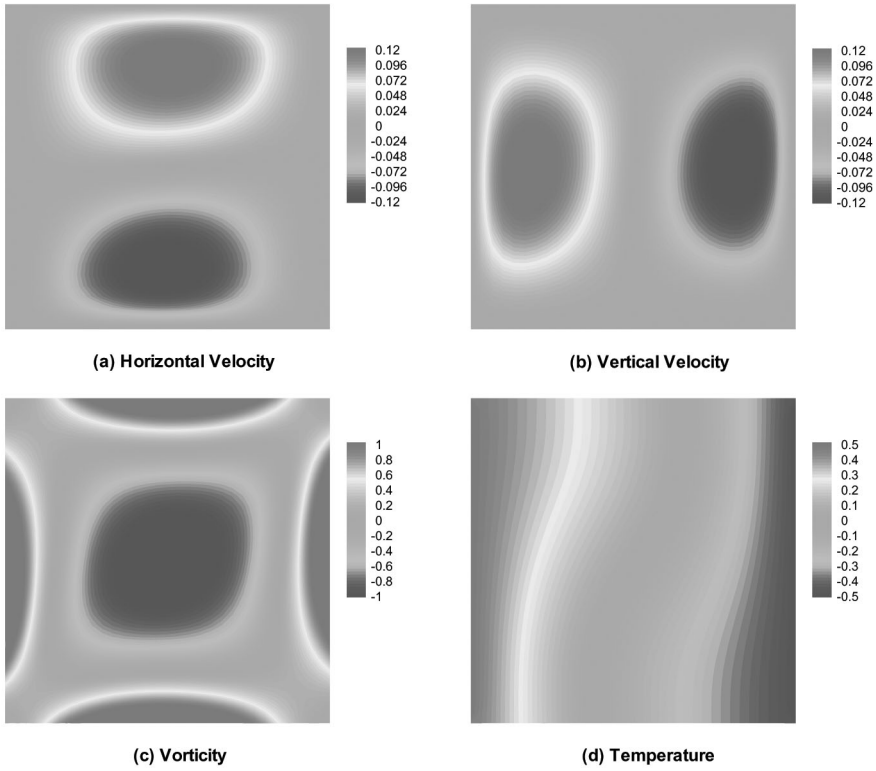

Figure 1.
Contour plots for the dependent variables at steady state in the square differentially-heated enclosure

computational fluid mechanicians for this problem and De Vahl Davis (1983) ran his own benchmark solution using a forward time, center space (FTCS) finite difference method. The current contour plots shown in Figure 1 are qualitatively similar to De Vahl Davis' contour plots.

In both papers De Vahl Davis (1983); by De Vahl Davis and Jones (1983), and benchmark solutions are provided for the maximum u-component of velocity along the vertical midplane of the enclosure, the maximum v-component of velocity along the horizontal midplane, and the average Nusselt number along either vertical side. The authors determined their benchmark solution by extrapolating results from a 11×11, 21×21, and 41×41 uniform finite difference mesh. The authors claimed that their benchmark solutions at a Rayleigh number of 1,000 were within 0.1 percent of the exact solution. However, the authors did not indicate what type of error measure they used or what type of analysis they used to arrive at their conclusion. A comparison of the current and the benchmark results is shown in Table I. The results generated with the vorticity method on both the 31×31 and 41×41 uniform mesh are in excellent agreement with the benchmark solutions. The percent

difference between all three sets of results for the maximum horizontal velocity, the maximum vertical velocity and the average Nusselt number are less than 1/2 of a percent.

4.2 Benchmark problem 2

As mentioned earlier, benchmark problem 2 considers an 8×1 differentially-heated enclosure at a near critical Rayleigh number of 310,000. This problem has been studied extensively and, in fact, was the topic of a series of special sessions at the First MIT Conference on Computational Fluid and Solid Mechanics (Christon *et al.*, 2001). Stability analyses indicate that the problem will reach a quasi-steady state, that is, the solution will oscillate about a mean (Salinger *et al.*, 2001). In the current results, a quasi-steady state is achieved after approximately 350 s when running the simulation from a quiescent state. Three separate discretizations are considered. The coarse discretization contained a 21×101 grid and used a dimensionless time step of 0.003. To resolve the boundary layers, the grid was stretched so that the finite elements were smaller near the walls of the enclosure. The minimum spacing of nodes in the x-direction was 0.01749 and the minimum spacing in the y-direction was 0.02938. The medium discretization contained a 41×201 stretched grid and also used a dimensionless time step of 0.003. The minimum spacing of nodes in the x-direction was 0.01471 and the minimum spacing in the y-direction was 0.01471. The fine discretization contained a 61×301 grid and used a dimensionless time step of 0.002. The minimum spacing in the x-direction was 0.00591042 and the minimum spacing in the y-direction was 0.00860986. The simulation for the fine mesh was not started from a quiescent state, but from the interpolated values of the medium mesh after quasi-steady state was reached. Interestingly enough, quasi-steady state in this case took approximately 180 s even though the initial conditions were fairly close to the quasi-steady state.

Contour plots for the principal unknowns, u, v, ω, and θ, generated using the medium discretization at a given instant in time are shown in Figure 2. The thermal and velocity boundary layers can easily be seen from the contour plots. The time histories of these unknowns at the point $x = 0.819$, and $y = 0.630$ are

Table I.
A comparison between the current vorticity and FTCS finite difference method results (De Vahl Davis, 1983; De Vahl Davis and Jones, 1983) for benchmark problem 1

	Vorticity method 31×31 mesh	Vorticity method 41×41 mesh	FCTS extrapolated results
u_{max}	0.1373	0.1373	0.1369
z	0.813	0.813	0.813
v_{max}	0.1392	0.1391	0.1387
$\underline{x}$	0.179	0.179	0.178
$\overline{\text{Nu}}$	1.117	1.116	1.118

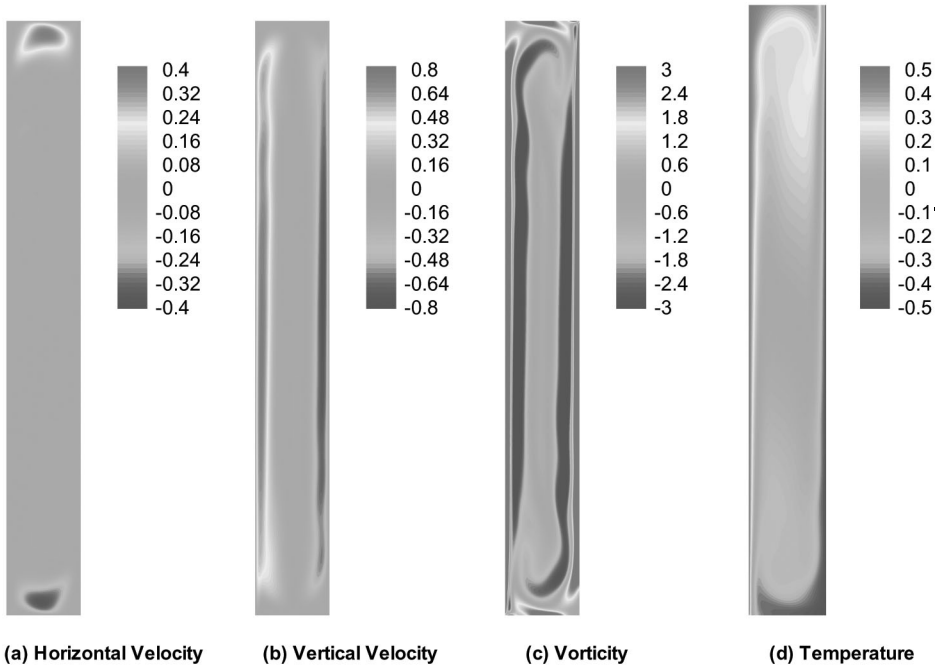

Figure 2.
Contour plots for the dependent variables at an instant in time for the 8×1 differentially-heated enclosure

shown in Figure 3 again using the medium discretization. As seen in the figure, quasi-steady state is achieved in approximately 350 s.

A quantitative comparison with benchmark data is provided in Table II. The benchmark data are provided by Xin and Le Quéré (1991) using a pseudo-spectral method and Johnston and Krasny (2001) using a vorticity-streamfunction method. The benchmark solutions were, in some sense, deemed to be the best solutions of approximately 30 contributions at the First MIT Conference on Computational Fluid and Solid Mechanics (Christon *et al.*, 2001).

The average values of the dependent variables u, v, ω, and θ are shown in the table for the point $x = 0.181$, and $y = 7.37$. The average Nusselt number, $\overline{\mathrm{Nu}}$, is integrated over the left-hand-side of the enclosure, although the value over the right-hand-side was found to be identical. The average kinetic energy and enstrophy are defined by

$$\hat{u}(t) = \sqrt{\frac{1}{2A}\int_A \vec{u}\cdot\vec{u}\,\mathrm{d}A};\ \hat{\omega}(t) = \sqrt{\frac{1}{2A}\int_A \omega^2\,\mathrm{d}A}.$$

The results for the point data generated by the vorticity code are seen to be approaching the benchmark results with grid refinement. The closest result is for the temperature which is within 2 percent of the benchmark result for the

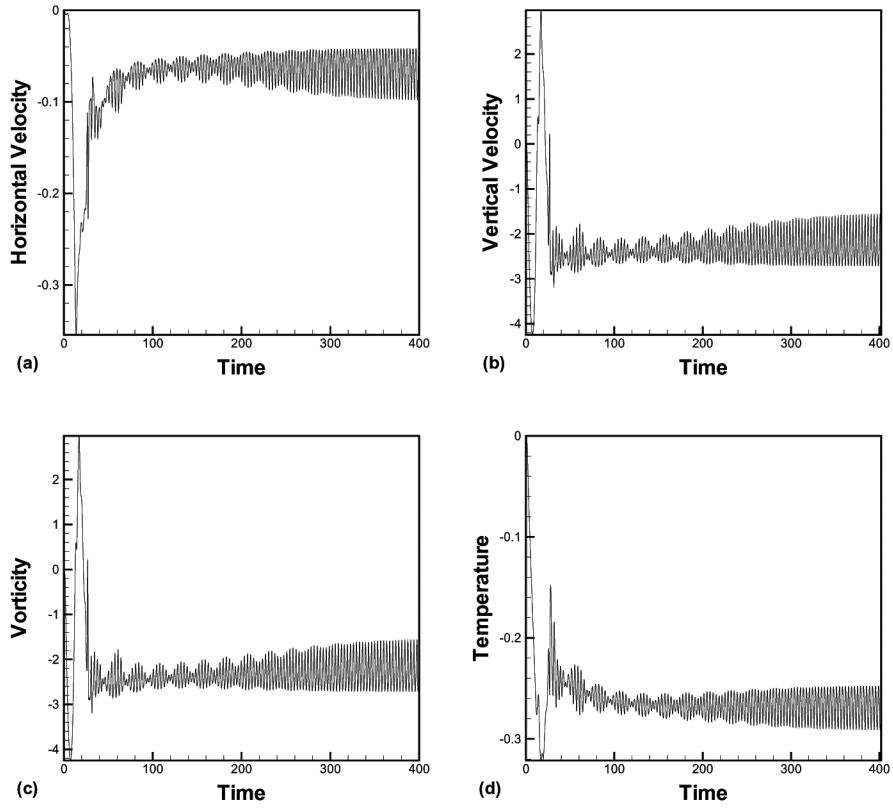

Figure 3.
Time histories of the dependent variables at the point $x = 0.819$, and $y = 0.630$

	Coarse grid	Medium grid	Fine grid	Benchmark solution
u	7.467E-2	6.448E-2	6.243E-2	5.636E-2[a]
Δu	8.449E-2	5.623E-2	4.179E-2	5.483E-2[a]
v	4.834E-1	4.776E-1	4.762E-1	4.583E-1[b]
Δv	9.670E-2	7.282E-2	5.630E-2	7.718E-2[b]
ω	−2.014	−2.220	−2.275	−2.362[b]
$\Delta\Omega$	1.836	1.158	8.608E-1	9.940E-1[b]
θ	2.678E-1	2.680E-1	2.697E-1	2.655E-1[a]
$\underline{\Delta\theta}$	6.579E-1	3.497E-1	3.280E-1	4.274E-1[a]
$\overline{\mathrm{Nu}}$	4.500	4.479	4.493	4.579[a]
$\hat{u}$	2.475E-1	2.446E-1	2.428E-1	2.389E-1[a]
$\Delta\hat{u}$	6.5E-5	3.9E-5	2.4E-5	1.683E-5[b]
$\hat{\omega}$	3.071	3.031	2.993	3.009[b]
$\Delta\hat{\omega}$	4.402E-3	3.186E-3	2.439E-3	1.608E-3[b]
Period	3.407	3.403	3.416	3.412[a]

Note: The benchmark solutions are provided by [a] Xin and Le Quéré (1991) and [b] Johnston and Krasny (2001)

Table II.
Comparison of the vorticity method solution with the benchmark solutions

fine mesh. The worse result is for the u-component of velocity which is only within 11 percent of the benchmark. However, the average speed at the test location ($\sqrt{u^2 + v^2}$) generated by the vorticity code is within 4 percent of the benchmark result. The match between the vorticity and benchmark results for the average values of the integrated quantities, namely, the Nusselt number, the average kinetic energy, and the enstrophy are much closer than the point data with the maximum difference being less than 2 percent.

All Δ quantities in Table II represent the peak-to-valley oscillation of the variable measured at quasi-steady state. The magnitudes of these oscillations are seen to decrease with grid refinement. For some reason, the Δ quantities generated using the medium mesh match the benchmark solutions better than the fine mesh results.

5. Conclusions

A vorticity formulation to analyze the natural convection of an incompressible, Boussinesque fluid in a differentially-heated enclosure has been developed. The vorticity formulation is based on a three-step algorithm in which the flow kinematics are governed by the GHD and the flow kinetics are governed by the vorticity and energy equations. The GHD is used to determine both vortex sheet strengths which yield Neumann boundary conditions for the vorticity equation and to determine the interior velocity field. In this way, the convective acceleration terms in both the vorticity and energy equations are linearized.

A novel Galerkin implementation of the GHD is presented. The Galerkin implementation not only provides far more accurate Neumann boundary conditions, but also has a couple of other practical advantages. First, the left-hand-side of the GHD is incorporated into the right-hand-side using rigid body arguments. This not only obviates the need of evaluating the coefficient $\eta(\vec{x})$ but also results in only double integrals appearing in the Galerkin GHD. Second, the Cauchy principal value integral appearing in the GHD has been regularized again using the rigid body arguments. Standard boundary element procedures are used to discretize both the regular and Galerkin form of the GHD.

Two benchmark problems are considered. The vorticity results at steady state matched extremely well to results available in the literature for the square enclosure at Ra = 1,000. The vorticity results for the 8×1 enclosure at Ra = 310,000 showed that a quasi-steady state is reached after approximately 350 s and that an unsteady oscillation with period of approximately 3.4 s appears in all the primary variables. Comparisons between the results generated with the current vorticity method and the benchmark numerical results agreed reasonably well especially for integrated quantities such as the Nusselt number, average kinetic energy, and average enstrophy.

References

Brebbia, C.A. and Dominguez, J. (1989), *Boundary Elements. An Introductory Course*, McGraw-Hill, New York.

Christon, M.A., Gresho, P.M. and Sutton, S.B. (2001), "Computational predictability of natural convection flows in enclosures", in Bathe, K.J. (Ed.), *Computational Fluid and Solid Mechanics*, Proceedings of the First MIT Conference on Computational Fluid and Solid Mechanics, Elsevier, Amsterdam, Vol. 2, pp. 1465-8.

De Vahl Davis, G. (1983), "Natural convection of air in a square cavity bench mark numerical solution", *Int. J. Num. Meth. Fluids*, Vol. 3, pp. 249-64.

De Vahl Davis, G. and Jones, I.P. (1983), "Natural convection in a square cavity: a comparison exercize", *Int. J. Num. Meth. Fluids*, Vol. 3, pp. 227-48.

El-Refaee, M.M. (1994), "Boundary layer control of separated flow over ircular cylinders – a BEM parametric study", *Eng. Anal. Bound. Elem.*, Vol. 14 No. 3, pp. 239-55.

Hribersek, M. and Skerget, L. (1996), "Iterative methods in solving Navier-Stokes equations by the boundary element method", *Int. J. Num. Meth. Eng.*, Vol. 39, p. 115.

Ingber, M.A. and Kempka, S.N. (2001), "A Galerkin implementation of the generalized Helmholtz decomposition for vorticity formulations", *J. Comp. Phys.*, Vol. 169, pp. 215-37.

Jeel, R., Škerget, L. and Petresin, E. (1999), "Natural convection in porous media: a numerical study of Brinkman model", in Brebbia, C.A. and Power, A. (Eds), *Boundary Elements XXI*, WIT Press, Southampton, pp. 145-54.

Johnston, H. and Krasny, R. (2001), "Computational predictability of natural convection flows in enclosures: a benchmark problem", in Bathe, K.J. (Ed.), *Computational Fluid and Solid Mechanics*, Proceedings of the First MIT Conference on Computational Fluid and Solid Mechanics, Elsevier, Amsterdam, Vol. 2, pp. 1486-9.

Kempka, S.N., Glass, M.W., Strickland, J.H. and Ingber, M.S. (1996), "Accuracy considerations for implementing velocity boundary conditions in vorticity formulations", Sandia National Laboratories Report SAND96-0583, Albuquerque, NM.

Koumoutsakos, P. and Leonard, A. (1995), "High-resolution simulations of the flow around an impulsively started cylinder using vortex methods", *J. Fluid Mech.*, Vol. 296, pp. 1-38.

Lighthill, M.J. (1963), "Chapter 11. Introduction: boundary layer theory", in Rosenhead, L. (Ed.), *Laminar Boundary Layers*, Oxford University Press, Oxford.

Machane, R., Achard, J-L. and Canot, E. (2000), "A new velocity-vorticity boundary integral formulation for Navier-Stokes equations", *Int. J. Num. Meth. Fluids*, Vol. 34, pp. 47-63.

Meir, A.J. and Schmidt, P.G. (1996), "Variational methods for stationary MHP flow under natural interface conditions", *J. Nonlin. Anal.*, Vol. 26 No. 4, p. 659.

Morino, L. (1986), "Helmholtz decomposition revisitied: vorticity generation and trailing edge condition", *Comput. Mech.*, Vol. 1, pp. 65-90.

Ostrikov, N.N. and Zhmulin, E.M. (1994), "Vortex dynamics of viscous fluid flows: Part 1. Two-dimensional flows", *J. Fluid Mech.*, Vol. 276, pp. 81-111.

Ramšak, M. and Škerget, L. (1999), "Mixed boundary elements for high RE laminar flows", in Brebbia, C.A. and Power, A. (Eds), *Boundary Elements XXI*, WIT Press, Southampton, pp. 453-62.

Salinger, A.G., Lehoucq, R.B., Pawlowski, R.P. and Shadid, J.N. (2001), "Understanding the 8:1 cavity problem via scalable stability analysis algorithms", in Bathe, K.J. (Ed.), *Computational Fluid and Solid Mechanics*, Proceedings of the First MIT Conference on Computational Fluid and Solid Mechanics, Elsevier, Amsterdam, Vol. 2, pp. 1497-500.

Tuncer, I.H., Wu, J.C. and Wang, C.M. (1990), "Theoretical and numerical studies of oscillating airfoils", *AIAA J.*, Vol. 28, pp. 1615-24.

Wang, C.M. and Wu, J.C. "A numerical study of general viscous flows around multi-element airfoils", *AIAA Paper No. 90-0572*.

Wu, J.C. and Thompson, J.F. (1973), "Numerical solutions of time-dependent incompressible Navier-Stokes equations using an integro-differential formulation", *Comput. Fluids*, Vol. 1, p. 197.

Xin, S. and Le Quéré, P. (1991), "An extended Chebyshev pseudo-spectral contribution to the CPNCFE benchmark", in Bathe, K.J. (Ed.), *Computational Fluid and Solid Mechanics*, Proceedings of the First MIT Conference on Computational Fluid and Solid Mechanics, Elsevier, Amsterdam, Vol. 2, pp. 1509-13.

Young, D.L., Yang, S.K. and Eldho, T.I. (2000), "Solution of the Navier-Stokes equations in velocity-vorticity form using a Eulerian-Lagrangian boundary element method", *Int. J. Num. Meth. Fluids*, Vol. 34, pp. 627-50.

Further reading

Batchelor, G.K. (1967), *An Introduction to Fluid Mechanics*, Cambridge University Press, Cambridge.